p-$BaSi_2$/n-Si heterojunction solar cells on Si(001) with conversion efficiency approaching 10%: comparison with Si(111)

Tianguo Deng, Takuma Sato, Zhihao Xu, Ryota Takabe, Suguru Yachi, Yudai Yamashita, Kaoru Toko, Takashi Suemasu*

Institute of Applied Physics, Graduate School of Pure and Applied Sciences, University of Tsukuba, Tsukuba, Ibaraki 305-8573, Japan

* Corresponding author.

Electronic mail: suemasu@bk.tsukuba.ac.jp

B-doped p-$BaSi_2$ epitaxial layers with a hole concentration of 1.1×10^{18} cm^{-3} were grown on n-Si(001) using molecular beam epitaxy to fabricate p-$BaSi_2$/n-Si solar cells. The thickness (*d*) of the p-$BaSi_2$ layer was varied from 20 to 60 nm to investigate its effect on solar cell performance. The conversion efficiency under AM1.5 illumination increased with *d* reaching a maximum of 9.8% at *d* = 40 nm, which is almost the same as the highest efficiency (9.9%) for p-$BaSi_2$/n-Si solar cells on Si(111). This work indicated that Si(001) substrates show promise for use in $BaSi_2$ solar cells.

A wide variety of materials have gained increasing attention for use in solar cells, including cadmium telluride, chalcopyrite, kesterite, and perovskite. These materials have allowed high conversion efficiencies (η) in low-cost solar cells. However, many of these materials contain rare and/or toxic elements. Therefore, finding effective absorber materials that are environmentally friendly is of great importance. Semiconducting orthorhombic barium disilicide ($BaSi_2$), composed of abundant elements, shows great potential as a solar cell material[1] as it has a suitable band gap of 1.3 eV[2,3] and a large absorption coefficient (α) of 3×10^4 cm^{-1} at 1.5 eV,[3-5] which is almost 40 times larger than that of crystalline silicon. A high η of over 25% is expected for a 2-μm-thick $BaSi_2$ homojunction solar cell.[6] In addition, alternative $BaSi_2$ containing solar cells have been proposed, such as $BaSi_2$ nanowires, back-contacted $BaSi_2$ solar cells and $BaSi_2$/perovskite stacked layers.[7-9] $BaSi_2$ can be grown epitaxially on a Si substrate[10,11] and its band gap can be increased by adding other elements such as Sr and C.[12,13] Thereby, $BaSi_2$ is a material of choice for targeting η > 30% in a Si-based tandem structure solar cell. As a first step, we chose to fabricate p-$BaSi_2$/n-Si heterojunction diodes on a flat n-Si(111) substrate, and achieved η values of 9.9%.[14] This is the highest η ever recorded for solar cells fabricated with semiconducting silicides. We have found that η was improved significantly by capping the p-$BaSi_2$ surface with an approximately 3-nm-thick amorphous Si (a-Si) layer.[15] These findings led to the recent success of $BaSi_2$ homojunction solar cells.[16] $BaSi_2$ containing solar cells are usually fabricated on Si(111) surfaces, even though the production of Si(001) substrates is far more abundant. We have used Si(111) substrates because $BaSi_2$ epitaxial films on Si(111) have exhibited a large minority-carrier lifetime (~10 μs), a large minority-carrier diffusion length (L~10 μm), and inactive grain boundaries.[17-20] In addition, the lattice mismatch is as large as approximately 1% for $BaSi_2$ on Si(111), which is much smaller than 12% for $BaSi_2$ on Si(001).[11] However, recent achievements in $BaSi_2$ on Si(001) such as large photoresponsivity and p-$BaSi_2$/n-Si solar cells have renewed interest in $BaSi_2$ on Si(001).[21-23] In this work, to explore the potential of Si(001) substrates for p-$BaSi_2$/n-Si heterojunction and

$BaSi_2$ homojunction solar cells, we fabricated p-$BaSi_2$ films on Si(001) substrates with thicknesses (d) ranging from 20 to 60 nm by molecular beam epitaxy (MBE). The hole concentration (p) was fixed at 1.1×10^{18} cm^{-3}. An η of 9.8%, which was comparable to the highest η obtained when fabricated on Si(111), was obtained at d = 40 nm under AM1.5 illumination. Moreover, both b and c-axis of the $BaSi_2$ films were under compressive strain, which was confirmed using Raman spectroscopy.

Samples were prepared using an ion-pumped MBE (R-DEC) system with a base pressure of less than 10^{-8} Pa, equipped with an electron-beam evaporation source for Si and standard Knudsen cells (K-cells) for Ba and B. These sample preparation procedures have been reported previously.[24] The p-type $BaSi_2$ epitaxial films (d = 20, 30, 35, 40, 50, and 60) were grown on n-Si(001) substrates (resistivity ρ = 1−10 Ωcm) and were named samples A–F, respectively. The crucible temperature of the B K-cell (T_B) was set at 1170 ºC to satisfy $p = 1.1 \times 10^{18}$ cm^{-3}. Subsequently, a 3-nm-thick a-Si capping layer was deposited on the $BaSi_2$ layers at 180 ºC to prevent oxidation of the $BaSi_2$ films.[25] The crystalline quality of films was characterized using reflection high-energy electron diffraction (RHEED) and X-ray diffraction (XRD; RIGAKU, Smart Lab) using Cu Kα radiation. The out-of-plane and in-plane XRD measurements gave the a, b, and c-axis lattice constants (a, b, and c) using the Nelson-Riely relationship.[26] A 440-nm-thick $BaSi_2$ film was used as a reference. Raman spectra were measured with a laser Raman spectrometer (JEOL, NRS-5100) with a frequency doubled Nd:YAG laser (532 nm). Surface morphologies were investigated using atomic force microscopy (AFM; Shimadzu SPM-9600). For optical characterization, an 80-nm-thick indium-tin-oxide (ITO) electrode (diameter = 1 mm) was sputtered on the front side and a 150-nm-thick Al electrode was sputtered on the entire back side. The current density versus voltage (J-V) characteristics under standard AM1.5 illumination and the photoresponse spectra were measured using a xenon lamp with a 25-cm-focal-length single monochromator (Bunko Keiki, SM-1700A and RU-60N). All measurements were performed at ambient temperature using a

mask with 1-mm-diameter holes, and the results were compared with those reported for devices fabricated on Si(111) substrates.[27]

The growth of the *a*-axis orientated p-$BaSi_2$ epitaxial films was confirmed for all samples using RHEED and XRD patterns. The *J-V* curves under AM1.5 illumination and external quantum efficiency (*EQE*) spectra for samples A–F are shown in Figs. 1(a) and 1(b), respectively. Solar cell behavior was observed for the devices fabricated on the Si(001) substrates in spite of the large lattice mismatch (~12%). The valence and conduction band offsets at the $BaSi_2$/Si interface, which is approximately 0.6 and 0.8 eV, respectively, promote the separation of photogenerated electrons and holes, as well as those in n-Si.[24] Equivalent data for p-$BaSi_2$/n-Si solar cells fabricated on Si(111) is shown in Figs. 1(c) and 1(d).[27] The solar cell performance of the devices fabricated on the Si(001) substrates changed depending on the value of *d*, with the largest η (9.8%) being obtained for sample D (*d* = 40 nm). This device exhibited a short-circuit current density (J_{SC}) of 37.0 mA/cm^2, an open-circuit voltage (V_{OC}) of 0.44 V, and a fill factor (*FF*) of 59.7%. The *J-V* curves (Fig. 1(a)) showed that the η improved for larger values of *d* initially, and then decreased because of a significant decrease in the J_{SC}. In addition, the V_{OC} almost saturated when $d > 30$ nm. The optimum *d* value for the p-$BaSi_2$/n-Si(111) solar cell was 20 nm (Fig. 1(c)).[27] The contribution of photogenerated carriers in the p-$BaSi_2$ layer decreased, especially in the short wavelength range, with increasing values of *d* (Figs. 1(b) and 1(d)). This indicated that it was difficult for the photogenerated minority carriers (electrons) in the p-$BaSi_2$ layer to reach the junction before recombination as *d* increased. This is attributed to a reduced *L* in the p-$BaSi_2$ films. Figure 1(e) presents the *EQE* spectra of p-$BaSi_2$/n-Si samples at *d* = 50 nm. Because α reaches 4×10^5 cm^{-1} at a wavelength of 500 nm in $BaSi_2$,[3] a large fraction of photons (>85%) at this wavelength are absorbed as they travel as far as 50 nm ($1/\alpha \times 2 = 50$ nm) through the p-$BaSi_2$ layer. The *EQE* values for sample on Si(001) are smaller than those on Si(111) especially in the short wavelength range, meaning that the *L* of the p-$BaSi_2$ on Si(001) is smaller than that on Si(111). We have already measured *L* values

of undoped $BaSi_2$ films on Si(111) and Si(001) by an electron-beam-induced-current (EBIC) technique, and they are 10 and 1.5 μm, respectively.[28] This difference in L comes from inactive grain boundaries of $BaSi_2$ on Si(111).[29] Although we have not evaluated L values of p-$BaSi_2$ films by EBIC, it is reasonable to consider that they are smaller for p-$BaSi_2$ on Si(001) than those on Si(111). Figure 1(f) shows the schematics of the band alignment of the diode simulated by automat for simulation of heterostructures (AFORS-HET).[30] The band bending occurs in the region close to the interface under illumination, marked by broken circles, and acts to disturb the transport of photogenerated electrons in the p-$BaSi_2$ to the n-Si region and photogenerated holes in the n-Si to the p-$BaSi_2$ region. This is caused by a small built-in potential of the diode (~ 0.2 V) because of a small electron affinity of $BaSi_2$ (3.2 eV).[31] Since such a band bending may limit the η of a p-$BaSi_2$/n-Si solar cell, we need to work on $BaSi_2$ homojunction solar cells to achieve much a higher η.

To accurately determine the reverse-bias saturation current density (J_0), shunt resistance (R_{SH}), and series resistance (R_S), we adopted a technique described by J. R. Sites and P. H. Mauk[32] and summarized in Fig. 2. Using the photodiode equation, the above parameters can be described using Eq. (1):

$$\frac{dV}{dJ} = SR_S + \frac{\gamma k_B T}{q}\left[\frac{1-(SR_{SH})^{-1}\,dV/dJ}{J + J_{SC} - (SR_{SH})^{-1}V}\right]. \quad (1)$$

Here, S is the device area, γ is the ideality factor of the diode, k_B is the Boltzmann constant, T is the absolute temperature, and q is the elemental charge. The J_0 decreased from 0.20 mA/cm^2 at d = 20 nm to 9.04 × 10^{-6} mA/cm^2 at d = 40 nm, which was comparable to the J_0 obtained for the p-$BaSi_2$/n-Si solar cell fabricated on Si(111) (J_0 = 1.39 × 10^{-5} mA/cm^2) with the highest η.[27] This result highlights the promise of $BaSi_2$ solar cells fabricated on Si(001) substrates. The decrease in the η at low values of d (20 and 30 nm, Fig. 2) was primarily caused by small FFs because of large R_S and small R_{SH}. To understand this decreased η at low d we examined the surface morphologies (5 μm × 5 μm) and cross-sectional profiles of p-$BaSi_2$ layers using AFM

for samples with d = 20, 40, and 60 nm, as shown in Fig. 3. These morphologies were examined before the deposition of the ITO surface electrode. The sample with d = 20 nm exhibited grain boundaries with gaps with depths of approximately 14 nm (Fig. 4(a)), showing that the entire Si surface was not covered by the film. The small R_{SH} calculated for this film likely originated from current leakage paths introduced as a consequence of direct contact between the ITO and the n-Si(001) substrate. At d = 40 and 60 nm, the n-Si(001) substrate was entirely covered with p-$BaSi_2$, resulting in the smaller J_0 and larger R_{SH} values. These results clearly demonstrated that contact of ITO and p-$BaSi_2$ and contact of p-$BaSi_2$ and n-Si have significant impacts on the values of R_{SH} and J_0. Conversely, a d of 20 nm was sufficient to cover the entire n-Si(111) surface, while d = 10 nm was not enough.[27]

The strains ($\Delta a/a$, $\Delta b/b$, and $\Delta c/c$), normalized using those of a reference sample with d = 440 nm, as functions of d on the Si(001) substrate are shown in Fig. 4(a). The equivalent graphs obtained on Si(111) substrates are presented in Fig. 4(b).[33] Surprisingly, the values of $\Delta a/a$, $\Delta b/b$, and $\Delta c/c$ were all negative when d was equal to or smaller than 60 nm. Their magnitude decreased monotonically and approached 0, which indicated that the $BaSi_2$ films were under compressive strain. In contrast, $\Delta a/a$ on the Si(111) substrate was positive and the dependence of the strain on d was more complicated (Fig. 4(b)). It is plausible that these differences in strain caused the different thicknesses of the p-$BaSi_2$ layer required to cover the entire n-Si surface when comparing Si(111) and Si(001) substrates. Raman spectra of the p-$BaSi_2$ films on the Si(001) substrate with different d values are shown in Fig. 4(c). Five Raman peaks were observed at wavenumbers below 500 cm^{-1},[34] denoted by F_g, E_g, $E_g + F_g$, F_g, and A_g, in addition to an intense peak (520.2 cm^{-1}) caused by the transverse optical phonon of Si (Si_{TO}) from the substrate. The Raman peaks F_g, E_g, and A_g originated from tetrahedral Si with T_h symmetry in the lattice of $BaSi_2$.[35] The peak positions in the Raman spectra as functions of d are shown in Fig. 4(d). As d increased, all peaks shifted to a smaller wavenumbers, which indicated that the films were under compressive stress in the in-plane direction.[36] This

compressive stress was consistent with the strains ($\Delta b/b < 0$ and $\Delta c/c < 0$) when considering the elastic stiffness constants of $BaSi_2$ using the elastic stress-strain relationship described by M. Grundmann.[37] As the Si *p* state appears dominant in the valence band maximum of $BaSi_2$ in both theory[4,5,38] and experiment,[39] it is possible that the stress introduced in the tetrahedral Si within the lattice modified the band structure of $BaSi_2$, leading to differences in its optical properties. Although further studies are required to verify the relationship between the induced stress and optical properties of $BaSi_2$, this work shows that Si(001) substrates are useful for $BaSi_2$ solar cells.

In summary, we fabricated B-doped p-$BaSi_2$/n-Si heterojunction solar cells on Si(001) substrates with different $BaSi_2$ layer thicknesses. We then examined the influence of the $BaSi_2$ thickness on the solar cells properties. The p-$BaSi_2$ films were found to be under compressive strain as well as compressive stress in the in-plane direction when $d < 60$ nm. The η reached a maximum value of 9.8% with a J_{SC} of 37.0 mA/cm^2, a V_{OC} of 0.44V, and a *FF* of 59.7%. These values were comparable to those obtained for devices fabricated on Si(111), indicating that Si(001) substrates can also be used for $BaSi_2$ solar cells.

This work was financially supported by JSPS KAKENHI Grant Numbers 15H02237 and 17K18865, and JST MIRAI. R.T. was financially supported by a Grant-in-Aid for JSPS Fellows (15J02139).

References

[1]T. Suemasu and N. Usami, J. Phys. D: Appl. Phys. **50**, 023001 (2017).

[2]K. Morita, M. Kobayashi, and T. Suemasu, Thin Solid Films **515**, 8216 (2007).

[3]K. Toh, T. Saito, and T. Suemasu, Jpn. J. Appl. Phys. **50**, 068001 (2011).

[4]D. B. Migas, V. L. Shaposhnikov, and V. E. Borisenko, Phys. Status Solidi (b) **244**, 2611 (2007).

[5]M. Kumar, N. Umezawa, and M. Imai, Appl. Phys. Express **7**, 071203 (2014).

[6]T. Suemasu, Jpn. J. Appl. Phys. **54**, 07JA01 (2015).

[7]A. Pokhrel, L. Samad, F. Meng, and S. Jin, Nanoscale **7**, 17450 (2015).

[8]R. Vismara, O. Isabella, and M. Zeman, Opt. Express **25**, A402 (2017).

[9]R. Vismara, O. Isabella, and M. Zeman, Proc. SPIE **9898**, 98980J (2016).

[10]R. A. McKee, F. J. Walker, J. R. Conner, E. D. Specht, and D. E. Zelmon, Appl. Phys. Lett. **59**, 782 (1991).

[11]R. A. McKee, F. J. Walker, J. R. Conner, and R. Raj, Appl. Phys. Lett. **63**, 2818 (1993).

[12]K. Morita, M. Kobayashi, and T. Suemasu, Jpn. J. Appl. Phys. **45**, L390 (2006).

[13]Y. Imai and A. Watanabe, Intermetallics **18**, 1432 (2010).

[14]S. Yachi, R. Takabe, H. Takeuchi, K. Toko, and T. Suemasu, Appl. Phys. Lett. **109**, 072103 (2016).

[15]R. Takabe, S. yachi, W. Du, D. Tsukahara, H. Takeuchi, K. Toko, and T. Suemasu, AIP Advances **6**, 085107 (2016).

[16]K. Kodama, R. Takabe, T. Deng, K. Toko, and T. Suemasu, to be published in Jpn. J. Appl. Phys. (2018).

[17]K. O. Hara, N. Usami, K. Nakamura, R. Takabe, M. Baba, K. Toko, and T. Suemasu, Appl. Phys. Express **6**, 112302 (2013).

[18]K. O. Hara, N. Usami, K. Toh, M. Baba, K. Toko, and T. Suemasu, J. Appl. Phys. **112**, 083108 (2012).

[19]M. Baba, K. Toh, K. Toko, N. Saito, N. Yoshizawa, K. Jiptner, T. Sekiguchi, K. O. Hara, N. Usami, and T. Suemasu, J. Cryst. Growth **348**, 75 (2012).

[20]M. Baba, M. Kohyama, and T. Suemasu, J. Appl. Phys. **120**, 085311 (2016).

[21]C. T. Trinh, Y. Nakagawa, K. O. Hara, R. Takabe, T. Suemasu, and N. Usami, Mater. Res. Express **3**, 076204 (2016).

[22]K. Takahashi, Y. Nakagawa, K. O. Hara, and N. Usami, Jpn. J. Appl. Phys. **56**, 05DB04 (2017).

[23]K. Takahashi, Y. Nakagawa, K. O. Hara, I. Takahashi, Y. Kurokawa, and N. Usami, MRS 2018 (doi.org/10.1557/adv.2018.191).

[24]D. Tsukahara, S. Yachi, H. Takeuchi, R. Takabe, W. Du, M. Baba, Y. Li, K. Toko, N. Usami, and T. Suemasu, Appl. Phys. Lett. **108**, 152101 (2016).

[25]R. Takabe, H. Takeuchi, W. Du, K. Ito, K. Toko, S. Ueda, A. Kimura, and T. Suemasu, J. Appl. Phys. **119**, 165304 (2016).

[26]J. B. Nelson and D. P. Riley, Proc. Phys. Soc. **57**, 160 (1945).

[27]S. Yachi, R. Takabe, K. Toko, and T. Suemasu, Jpn. J. Appl. Phys. **56**, 05DB03 (2017).

[28]M. Baba, K. Watanabe, K. O. Hara, K. Toko, T. Sekiguchi, N. Usami, and T. Suemasu, Jpn. J. Appl. Phys. **53**, 078004 (2014).

[29]M. Baba, M. Kohyama, and T. Suemasu, J. Appl. Phys. **120**, 085311 (2016).

[30]R. Varache, C. Leendertz, M. E. Gueunier-Farret, J. Haschke, D. Muñoz, and L. Korte, Sol. Energy Mater. Sol. Cells **141**, 14 (2015).

[31]T. Suemasu, K. Morita, M. Kobayashi, M. Saida, and M. Sasaki, Jpn. J. Appl. Phys. **45**, L519 (2006).

[32]J. R. Sites and P. H. Mauk, Solar Cells **27**, 411 (1989).

[33]Y. Yamashita, S. Yachi, R. Takabe, T. Sato, M. Emha Bayu, K. Toko, and T. Suemasu, Jpn. J. Appl. Phys. **57**, 025501 (2018).

[34]H. Peng, C. L. Wang, J. C. Li, R. Z. Zhang, M. X. Wang, H. C. Wang, Y. Sun, and M. Sheng, Phys. Lett. A **374**, 3797 (2010).

[35]Y. Terai, H. Yamaguchi, H. Tsukamoto, N. Murakoso, M. Iinuma, and T. Suemasu, Jpn. J. Appl. Phys. **56**, 05DD02 (2017).

[36]L. Yang, X. Cui, J. Zhang, K. Wang, M. Shen, S. Zeng, S. A. Dayeh, L. Feng, and B. Xiang, Sci. Rep. **4**, 5649 (2014).

[37]M. Grundmann, The Physics of Semiconductors, 3rd ed. (Springer, Berlin, Heidelberg, 2016), Chap. 5.

[38]Y. Imai and A. Watanabe, Intermetallics **10**, 333 (2002).

[39]M. Baba, K. Ito, W. Du, T. Sanai, K. Okamoto, K. Toko, S. Ueda, Y. Imai, A. Kimura, and T. Suemasu, J. Appl. Phys. **114**, 123702 (2013).

Figure captions

Fig. 1. *J-V* curves and *EQE* spectra of the p-$BaSi_2$/n-Si solar cells on Si(001) substrates ((a) and (b), respectively) and on Si(111) substrates ((c) and (d), respectively). (e) *EQE* spectra of the p-$BaSi_2$/n-Si solar cells on Si(001) and Si(111) substrates at d =50 nm in (b) and (d). (f) Schematics of calculated band alignments of a p-$BaSi_2$ (50 nm)/n-Si solar cell during short-circuit condition (left) and open-circuit condition (right) by AFORS-HET. E_C and E_V denote the conduction-band minimum and the valence-band maximum, respectively.

Fig. 2. Solar cell parameters (η, V_{OC}, J_{SC}, FF, R_S, R_{SH}, and J_0) of p-$BaSi_2$/n-Si solar cells formed on Si(001) and on Si(111)[27] substrates determined through calculations using Eq. (1).

Fig. 3. AFM images (5 μm×5 μm) and cross-sectional profiles (along the white line) of p-$BaSi_2$ layers from samples (a) A, (b) D, and (c) F.

Fig. 4. Normalized strains ($\Delta a/a$, $\Delta b/b$, and $\Delta c/c$) as functions of p-$BaSi_2$ thickness grown on (a) Si(001) and (b) Si(111).[33] (c) Raman spectra of p-$BaSi_2$ films on n-Si(001). (d) Raman peak positions as functions of thickness for the p-$BaSi_2$ films.

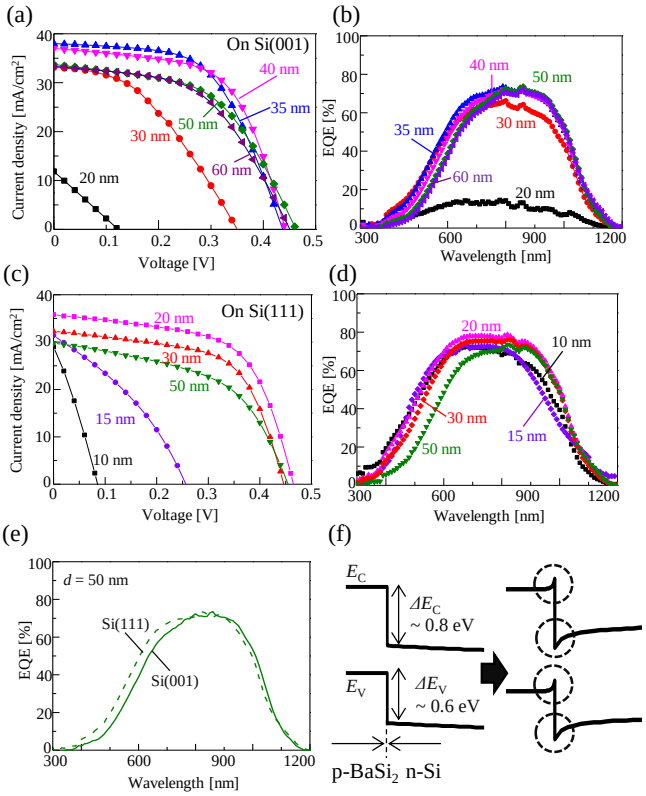
(a)
On Si(001)
40 nm
35 nm
50 nm
30 nm
60 nm
20 nm
Current density [mA/cm²]
Voltage [V]
(b)
40 nm
50 nm
35 nm
30 nm
60 nm
20 nm
EQE [%]
Wavelength [nm]
(c)
On Si(111)
20 nm
30 nm
50 nm
15 nm
10 nm
Current density [mA/cm²]
Voltage [V]
(d)
20 nm
10 nm
30 nm
15 nm
50 nm
EQE [%]
Wavelength [nm]
(e)
d = 50 nm
Si(111)
Si(001)
EQE [%]
Wavelength [nm]
(f)
E_C
ΔE_C
~ 0.8 eV
E_V
ΔE_V
~ 0.6 eV
p-BaSi2 n-Si

Fig. 1

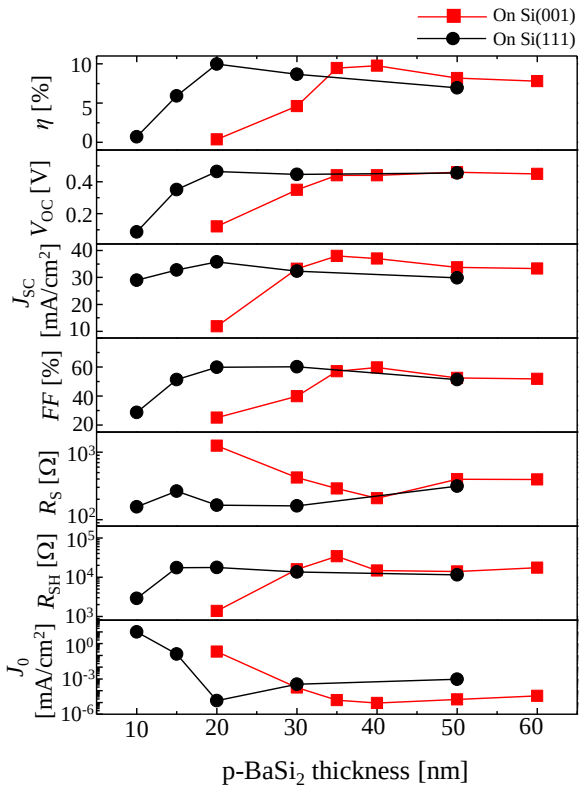
On Si(001)
On Si(111)
η [%]
V_OC [V]
J_SC [mA/cm²]
FF [%]
R_S [Ω]
R_SH [Ω]
J_0 [mA/cm²]
p-BaSi2 thickness [nm]

Fig. 2

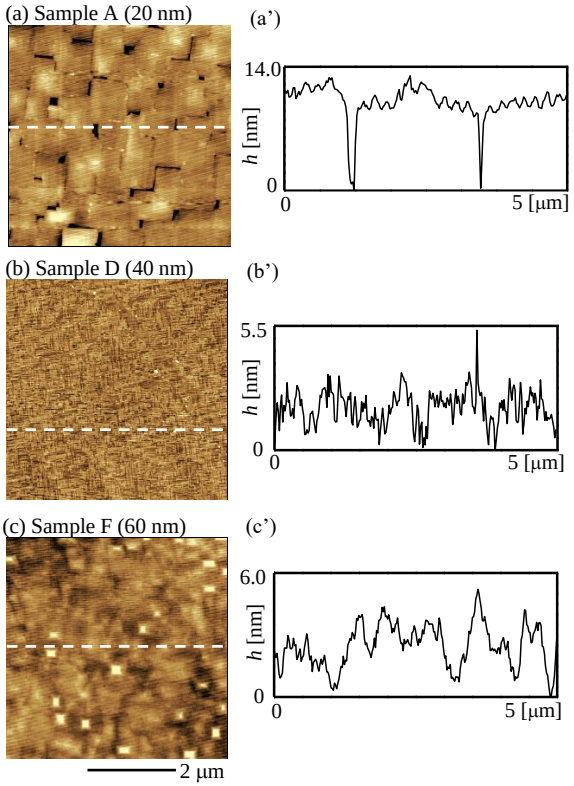
(a) Sample A (20 nm)
(a')
14.0
h [nm]
0
0
5 [μm]
(b) Sample D (40 nm)
(b')
5.5
h [nm]
0
0
5 [μm]
(c) Sample F (60 nm)
(c')
6.0
h [nm]
0
0
5 [μm]
2 μm

Fig. 3

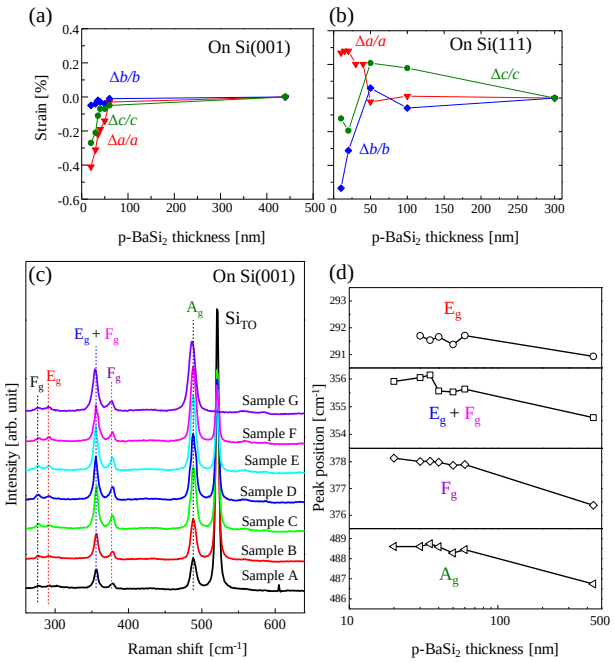
(a)
On Si(001)
Δb/b
Δc/c
Δa/a
Strain [%]
p-BaSi2 thickness [nm]
(b)
On Si(111)
Δa/a
Δc/c
Δb/b
p-BaSi2 thickness [nm]
(c)
On Si(001)
Ag
SiTO
Eg + Fg
Fg Eg
Fg
Sample G
Sample F
Sample E
Sample D
Sample C
Sample B
Sample A
Intensity [arb. unit]
Raman shift [cm-1]
(d)
Eg
Eg + Fg
Fg
Ag
Peak position [cm-1]
p-BaSi2 thickness [nm]

Fig. 4